Surface Shape Capture with Boundary Electrodes

Adam G. Kirk[1], Christine C. Ho[2]
[1]Dept. of Electrical Engineering and Computer Science
[2]Department of Material Science
University of California at Berkeley
Berkeley, CA, USA
[1]adam.g.kirk@gmail.com, [2]ho.christine.c@gmail.com

David Garmire
Department of Electrical Engineering
University of Hawai`i at Mānoa
Honolulu, HI, USA
david.garmire@gmail.com

***Abstract*— A system is proposed for monitoring changes in surface shape that is portable, inexpensive, durable, and works in many places where traditional shape monitoring techniques would fail. This system is ideally suited to monitoring large-scale surface deformations on surfaces like cloth without excessive wiring or the need for special purpose equipment. It is composed of a semiconductor-insulator-semiconductor sandwich of carbon-loaded polymer and unloaded polymer with electrodes attached at the boundary. The electrical properties of the material are sampled by applying currents and measuring resulting voltages at the boundary electrodes. The piezoresistive and geometry changes of the semiconductor layers results in resistance variations across the surface according to local curvature. Through sufficient sampling, a system of equations can be solved for the interior curvature properties. The local curvature data is integrated to yield an approximation of the surface shape. Various results are given that demonstrate the feasibility of the sensor with a prototype device.**

I. INTRODUCTION

There is a large and diverse demand for monitoring the shape of a surface in the areas of motion capture and user-interface devices [1]. Practical applications driving demand include activity monitoring for the elderly, soldiers, and first responders, augmented reality interfaces, sports medicine and physical therapy, and alternative input methods for gaming systems and smart phones. Prior methods that capture surface shape include motion capture rooms [2], light detection and ranging (LIDAR) [3], stereovision [4], and specially manufactured electrodes in the material (virtual-reality gloves and clothes [5]). Motion capture rooms and LIDAR currently are prohibitively expensive for general and personal use. LIDAR and stereovision have difficulties with handling occlusions due to line-of-sight constraints, absorbing materials, and low-level illumination.

Techniques most similar to our approach include placing on gloves or clothes piezoresistive strips [5], resistivity changing strips, or other strain-gauge sensor technologies [6][7]. Piezoresistive strips by themselves appear to suffer from high noise levels due to common-mode noise potentially stemming from wiring constraints and triboelectric or electromechanical interaction of the materials. There are also calibration issues if directly embedded in cloth due to difficulty in controlling layer thickness and interactions between the textile and strain-gauge materials. Strain-gauge approaches to-date focus on using a single strain gauge in a linear fashion. To extract curvature over a surface, several strain gauges need to be placed at orthogonal angles to each other. These approaches then have the difficulty that the number of electrodes and attached wires scales linearly with the number of strain gauges. Unfortunately, highly conductive lines are costly to make both flexible and durable [8], and processing to add in numerous lines to a sheet can both affect the mechanical bending properties of the surface and drive up manufacturing cost.

The proposed system contains a single sheet to reduce the requirements on wiring. While a single strain-gauge layer is sufficient for determining purely stretching modes of the sheet, a double strain-gauge layer is shown to be ideally suited for determining curvature of the sheet of material. The differential change in resistivity between the top and bottom layers is exploited to reduce common-mode noise and more accurately determine the curvature change of the sheet. Internal local curvature can be determined by solving a set of equations from supplying multiple currents and measuring resulting voltages at the boundary electrodes. The number of electrodes then scales linearly to the perimeter length and desired resolution reducing manufacturing complexity. However, linearly more currents also need to be supplied for every sampling time placing more constraints on the speed of the hardware. Fortunately for human motion capture, sampling time is not the limiting factor as the shortest motions of interest are typically in the 10-100 ms range [9].

Because this sensor is inexpensive, easy to fabricate, and does not require a calibrated environment, it is well suited to a wide range of applications. Examples of such applications include user input and safety monitoring. One can imagine wearing clothing with these sensors embedded, which would enable the user to interact with devices using only gestures. Alternatively, interested parties could monitor the behavior of people or objects in high stress environments.

II. THEORY

The bending of a layer of material results in the expansion of the material on one side and compression of the material on the opposite side. In Fig. 1, t is the total layer thickness, h is the semiconductor layer thickness (and $h << t$), L is a unit length, W is a unit width, R is the radius of curvature, and κ is the curvature. By convention, "d" before a symbol denotes the change in that quantity due to deformation, "δ" before a symbol, x, means dx/x, a subscript "L" or "W" after a quantity indicates its direction is either in the lengthwise or lateral direction respectively, and a superscript "T" or "B" after a quantity indicates it belongs to the top or bottom semiconductive surfaces respectively. By similar triangles, it is clear that for small amounts of bending, the strain in the lengthwise direction, $\varepsilon_L = dL/L$, is related to R_L, κ_L, and t as

$$\varepsilon_L = \delta L = \frac{dL}{L} = \frac{t}{2R_L} = \frac{t}{2}\kappa_L . \quad (1)$$

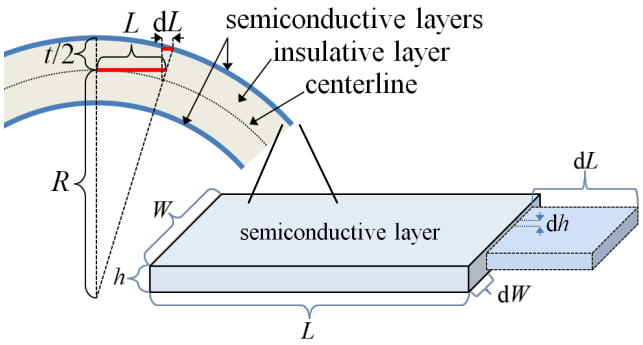

Figure 1. Bending of a layer of material stretches the top surface and compresses the bottom surface. The stretched layer (inset) contracts in the lateral and out-of-plane directions according to Poisson's ratio, υ.

Strain in one direction of the material typically results in deformation in the orthogonal directions according to Poisson's ratio, υ. Also the resistivity of the material, ρ, may change as a function of induced strain due to the piezoelectric effect that is usually linearized in a strain-gauge factor, G, as $\rho' = \rho(1 + G\varepsilon)$. Temperature effects are ignored in this analysis because they similarly affect the bottom and top layers. The resistance of the unit of material in the lengthwise direction, $\Re_L = \rho_L \frac{L}{hW}$, is changed as follows for small strains:

$$L' = L(1+\varepsilon_L), W' = W(1-\upsilon\varepsilon_L), h' = h(1-\upsilon\varepsilon_L), \quad (2)$$

$$\Re_L' = \rho_L' \frac{L'}{h'W'} \approx \Re_L\left(1+(1+2\upsilon+G)\varepsilon_L\right) \ (\varepsilon_L). \quad (3)$$

The resistance in the lateral direction, $\Re_W$, is affected also:

$$\Re_W' = \rho_W' \frac{W'}{h'L'} = \Re_W\left(1-(1+G\upsilon)\varepsilon_L\right). \quad (4)$$

Considering a sheet of material, we can subdivide the sheet according to an arbitrary internal grid that will be useful in discretizing the real-valued resistance of the sheet in the L and W directions, $\Re_L(x,y)$ and $\Re_W(x,y)$, and relating those to local curvatures, $\kappa_L(x,y)$ and $\kappa_W(x,y)$, through (3) and (4) using the additive nature of deformations. The resulting local matrix equation for the top surface is:

$$\begin{bmatrix} \delta\Re_W^T \\ \delta\Re_L^T \end{bmatrix} = \frac{t}{2}\begin{bmatrix} (1+2\upsilon+G) & -(1+G\upsilon) \\ -(1+G\upsilon) & (1+2\upsilon+G) \end{bmatrix}\begin{bmatrix} \kappa_W \\ \kappa_L \end{bmatrix}. \quad (5)$$

Similarly, the bottom-surface resistance changes should be close to equal and opposite to the top-surface resistivity changes ($\delta\Re_W^B = -\delta\Re_W^T$ and $\delta\Re_L^B = -\delta\Re_L^T$) even for differences in the thickness of the semiconductive-layer ($h^B \neq h^T$) as long as the centerline of bending remains close to $t/2$.

A. Solving Resistances from Boundary Measurements

We represent the sheet in an equivalent circuit as a regular grid of nodal points with lengthwise and lateral resistors (Fig. 2). Nodal voltages are labeled $V_{i,j}$, $i = 1..n$, $j = 1..n$, and n is the number of boundary electrodes along a side (for simplicity we assume the same number in the horizontal and vertical directions). Additionally, the voltages will be different for every set of supplied boundary currents so an additional index, k, in $V_{i,j,k}$ denotes the k^{th} current configuration. The resistances between nodes are represented as $\Re_{i,j,u}$, $\Re_{i,j,l}$, $\Re_{i,j,r}$, and $\Re_{i,j,d}$ for the resistor above, to the left, right, and below node (i, j) respectively. The interior voltages are not initially known and must be solved for each set of supplied currents simultaneously with the resistances between nodes.

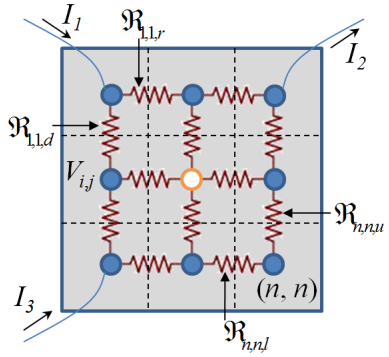

Figure 2. Representation of an equivalent circuit superimposed on a sheet of material. Note that three current pathways are supplied in this example.

Due to the nonlinear nature of simultaneously solving for unknown voltages, currents, and resistances, a nonlinear fitting routine is employed that can be iteratively updated using the solution from the previous time step to reduce computational cost. A simplifying result is that once the initial resistances are solved, it is only necessary to solve for the change in resistances ($\delta\Re$) and we know from our prior analysis that the change in resistance of the top resistors

should be negative the change in the corresponding bottom resistors. Kirchhoff's Current Law (KCL) provides a set of equations that need to be satisfied at each nodal point – the currents into each node must be equal to the currents out of the node. For a given estimate of resistances and interior voltages, a non-zero residual current, $I^{res}_{i,j,k}$, is the error where

$$I^{res}_{i,j,k} = \frac{V_{i,j,k}-V_{i-1,j,k}}{\Re_{i,j,l}} + \frac{V_{i,j,k}-V_{i+1,j,k}}{\Re_{i,j,r}} + \frac{V_{i,j,k}-V_{i,j+1,k}}{\Re_{i,j,d}} + \frac{V_{i,j,k}-V_{i,j-1,k}}{\Re_{i,j,u}} \quad (6)$$

The number of terms in (6) will depend on the location of the node (boundary, interior, or at the location of a supplied current). An additional constraint that needs to be enforced is the interior geometry. Assuming the sheet resistance is relatively uniform, an appropriate way to enforce geometry of the interior mesh is to also reduce the residuals $1/\Re_{i,j,u} - 1/\Re_{i,j,d}$ and $1/\Re_{i,j,l} - 1/\Re_{i,j,r}$. Finally, additional residual terms can be added to aid in convergence of the chosen nonlinear fitting routine by not allowing resistances to grow too small or too large. We chose MATLAB's nlinfit which uses an algorithm based on Gauss-Newton with Levenberg-Marquardt modifications [10] as the nonlinear solver. The appropriate number of supplied sets of currents, K, is found from the number of unknowns in the system, $4n(n\text{-}1)+2K(n\text{-}2)^2$, and the number of equations from KCL, $2Kn^2$. A unique solution requires that $K \geq n/2$ for large n; however, more sets are preferred to ensure robustness. We then solve for local curvature at each nodal location using (5).

B. Solving Global Shape from Local Curvatures

The curvatures obtained at each node in the previous section describe the local behavior of the surface at that point. Given the curvature information and relative location of each node, we can obtain the three-dimensional shape of the material. Lipman et al. [11] describe a method to integrate local surface information to obtain a mesh representing the global surface in two steps. First, they construct a local coordinate frame at each node point, after which they solve for the transformation between that coordinate frame and those at the neighboring nodes. We follow a similar approach.

The first step is to build a local surface patch at each node. By construction, we know the location of every node with respect to every other in the default configuration. If we assume that the material does not shear as easily as it wrinkles, we can assume that the majority of the local curvature is due to out-of-plane motion and so we can build a local surface patch by integrating the local curvature inside the patch, while ensuring that the arclength between nodes stays the same. More specifically, for each topological node v_i, we consider its neighbors $v_{i,j}$. These neighbors define the neighborhood of v_i (Fig. 3). The curvatures in the previous section are defined relative to the default configuration (as are the default neighboring node locations), which gives us the ability to determine local surface shape by integrating the curvature along each edge from v_i to $v_{i,j}$. Essentially, we are bending the edge from v_i to $v_{i,j}$ in the plane $(v_{i,j} - v_i) \times \mathbf{n}_i$ (where $\mathbf{n}_i$ is the normal at v_i) such that it fits the curvature from the previous section, then representing the surface patch as vectors from v_i to the end point of the bent edge. We numerically integrate the patch curvature along each edge as out-of-plane deformation to compute the end point of the bent edge.

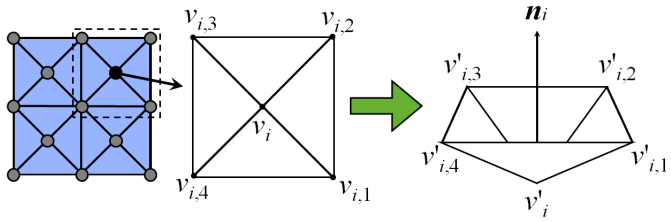

Figure 3. Node positions and normal vectors are updated using the local curvature information. See end of Section V for creating a triangular mesh from a quadrilateral mesh used in determining local curvature.

After performing this procedure for every node, we have a collection of local surface meshes that need to be oriented relative to each other to create a global surface mesh. To do this, note that we know $\mathbf{n}_i$ in the local surface mesh centered on v_i. We also can determine $\mathbf{n}_{i,j}$, which is the normal to vertex $v_{i,j}$ expressed relative to $\mathbf{n}_i$. From the edges and the normals, we can build a coordinate frame for v_i as well as a coordinate frame for $v_{i,j}$ relative to v_i. At this point, we have coordinate frames for each node as well as relative definitions of neighboring coordinate frames. A global surface mesh results from integrating these relative coordinate frames. For details on solving for the global surface mesh, see [11].

III. DEVICE

The sandwich of semiconductor and insulator layers (also referred to as a bi-conductive sheet) is required to be highly flexible so that it can sit on cloth without adding excessive mechanical resistance. This requirement limits the choice of materials to elastomeric compounds. We use Sylgard® 184 polydimethylsiloxane (PDMS) as our base polymer and insulative layer. Our recipe for carbon-loaded PDMS (cPDMS) consists of 5:1 Acetylene Black:PDMS by weight, plus 7.5 mL toluene per gram of Acetylene Black. The cPDMS is first prepared, sonicated, and bladed across a Kapton sheet to ensure uniform thickness. The material is cured in an oven for 2 hours at 100° C. Then, a layer of PDMS is bladed across the cured cPDMS and also cured. Finally, two squares of this material are cut and placed on each other. Another layer of PDMS is added between these two layers for bonding them and this sheet is completely cured. The sheet is then wired and prepared for testing (Fig. 4).

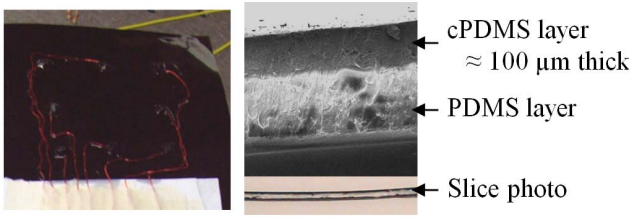

Figure 4. A processed device (left) and cross-sections of different slices of bi-conductive material (right)

IV. RESULTS

For all results, a National Instruments USB-6259 data acquisition box was used to apply and measure voltages to the devices. Using van der Pauw's method [13], sheet resistance of a 110 ± 10 µm thick cPDMS square (8 cm on a side) with corner electrodes was measured to be 814 ± 16 Ω (100 samples). The resistivity of the cPDMS layer is then 0.0895 ± 0.0083 Ω·m giving a conductivity of 11 ± 1 S·m^{-1} and placing it within the range of other forms of carbon [14]. Dopant concentrations could be added and would likely enhance the piezoresistive response; however without doping, negligible Gauge factor was assumed due to piezoresistivity except for that which may be inherent to a carbon loaded polymer matrix [15].

From the bi-conductive sheet, two tests were run. In the first test (Fig. 5), a linear curvature sensor was made using a single layer of the cPDMS embedded on a glove and compared with a linear curvature sensor made using a strip of the bi-conductive sheet. The single layer of cPDMS was probed using a voltage divider technique with a supplied voltage of 10 V and an external 1 MΩ resistor in series. The bi-conductive sheet was probed by supplying a 10 V signal to both ends and measuring the differential voltage drop at a point before the bend of the knuckle. In both cases, the strips were attached to the glove using PDMS. The plotted results were randomly selected and unprocessed voltages.

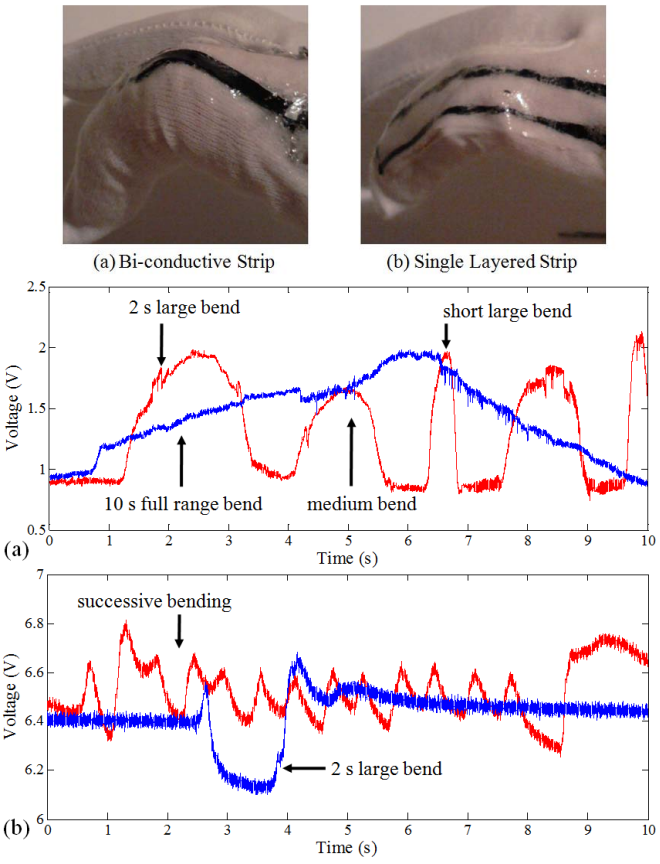

Figure 5. Comparison of bending response in (a) a bi-conductive strip and (b) a single-layered strip. (b) can be compared with other measurements [5]

The second test was instrumenting a square piece of the sheet material with electrodes on the top and bottom surfaces in a square pattern according to Fig. 6. The wires were attached to the surface using cPDMS as the bonding agent. It was found that other fastening techniques such as soldering and using nickel-loaded PDMS were not as good in durability and in decreasing contact resistance. The test used $n = 3$ for the number of electrodes on a side. Three different current sets were cycled every 2 ms.

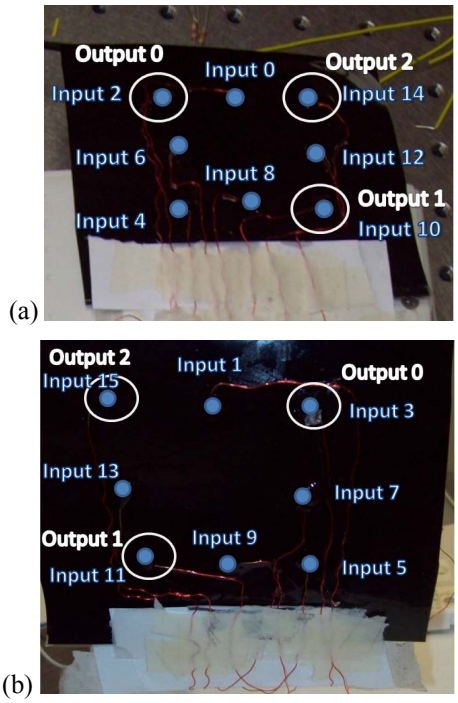

Figure 6. Wiring of the device showing (a) the top electrodes and (b) the bottom electrodes.

The sheet was tested under multiple bending modes including bending the middle of the far edge of the sheet downwards (Fig. 7) and bending the far corner of the sheet upwards and off-axis (Fig. 8). Applying these two bending modes tested whether the system could tell the difference between them. As described in the Theory section, the initial resistances and voltages of the network were solved using nlinfit (the nonlinear fitting function MATLAB) on the equations from KCL. From there, changes in resistances were solved using the fact that the change in the resistances of the top sheet would be equal and opposite to the corresponding change in resistances in the bottom sheet, or differ by a common factor, α, in the worst case (due to bending variations from the centerline shown in Fig. 1). α was a parameter solved for in the fitting routine. Local curvature was found by using these changes in resistances in solving (6). From local curvature, the global shape was extracted according to Section II.B. Finally the extracted shape was compared with digital video taken of the sample being bent. The result shows conceptual agreement for both modes tested; however, there are some variations especially under large deformation as in the corner-bending case (Fig. 8) that results in exaggerated bending in the corner nodes.

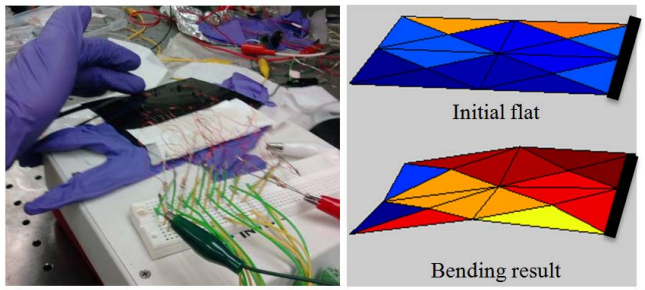

Figure 7. Bending the sheet in the center produced the reconstructed surface result to the right (the initial flat is in the same orientation as the result).

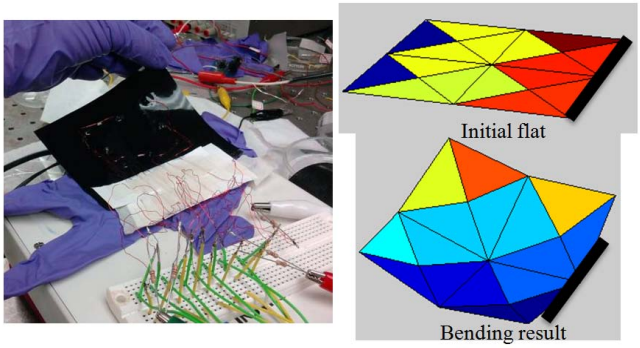

Figure 8. Bending the sheet in the far corner produced the reconstructed surface to the right (the initial flat is in the same orientation as the result).

In terms of durability, a bi-conductive sheet has been subjected to approximately 1000 high curvature bends in a wallet. No degradation is apparent. This result stands to reason considering carbon black is the main additive used to increase the lifetime of rubber tires.

V. Discussion

These results show that a bi-conductive sheet has a higher signal-to-noise ratio (SNR) and lower drift than an equivalent single-layered sheet (Fig. 5) as well as more directly mapping to the curvature in the finger. In the single layer sheet, it is unclear how the voltage change relates to the curvature change in the finger and it has slow transient characteristics (Fig. 5 blue line between seconds 4 and 6). It is likely that the drift is taken care of in the bi-conductive sheet by the differential voltage measurement. The correlated noise should also be reduced due to the differential pathway along the top and bottom conductive layers. However, the noise level in both devices appears to be around an RMS of 11 mV and the SNR in the bi-conductive sheet is 127 compared to the SNR of 51 for the single layer. It appears that the signal in the bi-conductive sheet is amplified by curvature change as compared to the single layer sheet which stands to reason because the top surface should increase resistance upon bending downwards while the bottom surface should decrease resistance. The noise is dominant at low frequencies with a peak around 60 Hz (as identified using MATLAB's spectrogram function), so it appears that the limiting noise source is due to inadequate shielding. Further noise shielding can be provided by surrounding the encapsulated strain gauges in an outer conductive layer, potentially made with cPDMS as well due to its strong adhesion to PDMS and high flexibility.

If the low frequency noise can be mitigated through proper shielding, it is worthwhile understanding how the two approaches would compare in the limiting case. Taking this noise analysis a step further, it is important to examine the circuits used to probe the resistance changes (Fig. 9). A pure resistance-based measurement such as in using a voltage divider has Johnson-Nyquist voltage noise (or thermal noise) on the order of $\sqrt{4k_BTR}$ where k_B is the Boltzmann's constant, T is the temperature, and R is the resistance [12]. For room temperature and the approximate 2 MΩ resistance in the single-layered strip of the glove, the thermal noise limit is approximately 0.13 mV. Thermal noise for an RC circuit on the other hand does not depend on resistance but rather on the capacitance due to filtering according to $\sqrt{k_BT/C}$ [13] (note that voltage-divider analysis would still apply to the common-mode noise which is rejected by measuring the differential voltage between the top and bottom layers). The capacitance of the bi-conductive strain gauge was measured to be 0.1 nF which corresponds to a noise of 0.006 mV.

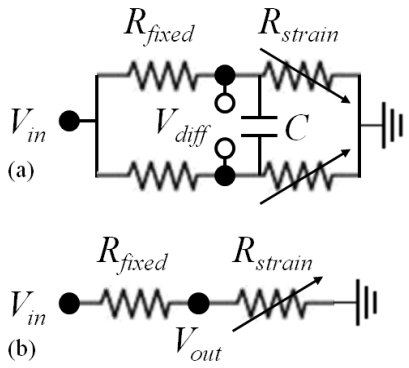

Figure 9. Probing circuits used in measuring the corresponding strain gauges in Fig. 5 for the (a) bi-conductive layer and (b) single layer.

Inaccuracies still are apparent in the differential measurement of the bi-conductive sheet in terms of sudden slight jumps (Fig. 5a blue line near the 4 second mark). These jumps appear to be a result of unintentional contacts being made as the sheet is actuated in the glove. They can likely be eliminated by securing all contacts.

While the current approach for surface shape capture employs a black-box nonlinear solver, the efficiency of solving the system can be improved both by knowing resistivities ahead of time and accurately predicting the next resistivities based on the continuity of the changes. A more tailored nonlinear solver could also help improve the solution time which is currently on the order of 1 second per time step (which requires off-line processing). The difficulty in solving for the resistivites lies in the bilinear equations. In this particular case, however, there is some amount of domain knowledge that can restrict the solution space, for example we have reasonable bounds on the range of resistivies and voltages. A tailored solver could take advantage of this knowledge. It may be possible to employ the approach of van

der Pauw [13] to determine a more direct approach to solving for the interior resistances; however, this method would need to be extended to the case of varying sheet resistivity and anisotropic resistivities.

Note that the topological configuration for the mesh representation is a triangulation of the surface, while the topology for the curvature solution from changes in resistances is a quadrilateral mesh. The surface is represented as a quadrilateral mesh during the curvature determination phase because the solution contains fewer variables (making the solve easier). In contrast, the surface mesh is represented as a triangular mesh because each facet is guaranteed to be planar, if the solution used a quadrilateral mesh there would need to be constraints to enforce planarity. The curvatures at the additional nodes in the triangulation are obtained through interpolation.

VI. Conclusion

This system demonstrates surface shape capture using boundary electrodes connected to a flexible sheet containing two carbon loaded polymer layers. Such a sensor has shown to be extremely durable and lightweight as well as inexpensive and easy to produce. Furthermore, the material is easy to apply to existing objects, such as a glove, or can be produced as a stand-alone sheet. In the one-dimensional case, the system is able to reliably detect the degree of actuation of a joint. Experiments show that the multi-layer structure outperforms a single layer in terms of noise. In the two-dimensional case, the system is able to determine the approximate degree of curvature of a sheet of material and, in particular, with just a few electrodes reliably determine convex versus concave shape. Taking additional samples and adding more electrodes will increase the resolution of the data.

This type of sensor is ideally suited to detecting large deformation without being constraining or obtrusive. There are many relevant applications, such as device interaction or industrial safety monitoring. Because the material can be applied directly to existing devices, it is possible to create sensing surfaces even on curved devices. For example, the non-display surfaces of a smartphone can be coated in this type of sensor, making the entire device interactive. These sensors could also be used for monitoring the shape of sails. A second motivating application is human behavioral and safety monitoring. In this case, the sensor can be embedded into clothing to provide data on the subject's actions. A combination of one and two-dimensional sensors can provide data used in discriminating actions and providing valuable feedback, as well as enabling the subject to interact with their digital environment via gesture.

Acknowledgment

The authors wish to thank Professor Paul K. Wright for the use of his laboratory space during the development of this project. The authors also thank Dr. Alejandro De la Fuente Vornbrock for discussions and consultations on the project.

References

[1] C. Mattmann, F. Clemens, G. Tröster, "Sensor for Measuring Strain in Textile", Sensors (MDPI), vol. 8 p. 3719-3732, 2008.

[2] M.S. Geroch, "Motion capture for the rest of us," J. Comput. Small Coll., vol. 19, 2004, pp. 157-164.

[3] R. Kolluri, J. R. Shewchuk, J. F. O'Brien, "Spectral Surface Reconstruction from Noisy Point Clouds", SGP 2004.

[4] R. White, K. Crane, D. Forsyth, "Capturing and Animating Occluded Cloth", ACM TOG (Siggraph) 2007.

[5] D. De Rossi, F. Carpi, F. Lorussi, A. Mazzoldi, R. Paradiso, E.P. Scilingo, and A. Tognetti, "Electroactive fabrics and wearable biomonitoring devices," AUTEX Research Journal, vol. 3, 2003, pp. 180–185.

[6] G. Harsányi, "Polymeric sensing films: new horizons in sensorics?," Materials Chemistry and Physics, vol. 43, Mar. 1996, pp. 199-203.

[7] A. Bonfiglio, D. De Rossi, T. Kirstein, I.R. Locher, F. Mameli, R. Paradiso, and G. Vozzi, "Organic field effect transistors for textile applications," IEEE transactions on information technology in biomedicine, vol. 9, 2005, pp. 319–324.

[8] T. Sekitani, H. Nakajima, H. Maeda, T. Fukushima, T. Aida, K. Hata, and T. Someya, "Stretchable active-matrix organic light-emitting diode display using printable elastic conductors," Nat Mater, vol. 8, Jun. 2009, pp. 494-499.

[9] A.F. Huxley, "Muscular contraction", The Journal of Physiology, vol. 243, 1974, pp. 1-43.

[10] C.T. Kelley, "Iterative methods for optimization", Society for Industrial Mathematics, 1999.

[11] Y. Lipman, O. Sorkine, D. Levin, D. Cohen-Or, "Linear Rotation-invariant Coordinates for Meshes", ACM Transactions on Graphics (Proceedings of ACM SIGGRAPH), pp. 479-487, 2005.

[12] H. Nyquist, "Thermal Agitation of Electric Charge in Conductors," Physical Review, vol. 32, Jul. 1928, p. 110.

[13] R. Sarpeshkar, T. Delbruck, and C.A. Mead, "White noise in MOS transistors and resistors," IEEE Circuits and Devices Magazine, vol. 9, 1993, pp. 23–29.

[14] L. J. Van der Pauw, "A method of measuring specific resistivity and Hall effect of discs of arbitrary shape", Philips Research Reports 13, pp. 1–9, 1958.

[15] P.J. Mather and K.M. Thomas, "Carbon black/high density polyethylene conducting composite materials: Part I Structural modification of a carbon black by gasification in carbon dioxide and the effect on the electrical and mechanical properties of the composite," Journal of materials science, vol. 32, 1997, pp. 401–407.

[16] J. Zhou, Y. Song, Q. Zheng, Q. Wu, and M. Zhang, "Percolation transition and hydrostatic piezoresistance for carbon black filled poly(methylvinylsilioxane) vulcanizates," Carbon, vol. 46, Apr. 2008, pp. 679-691.